Energy & Environmental Science

Cite this: *Energy Environ. Sci.*, 2012, **5**, 6500

www.rsc.org/ees

PAPER

Highly durable SiOC composite anode prepared by electrodeposition for lithium secondary batteries†

Hiroki Nara, Tokihiko Yokoshima, Toshiyuki Momma and Tetsuya Osaka*

Received 24th November 2011, Accepted 17th January 2012
DOI: 10.1039/c2ee03278c

A highly durable SiOC composite anode was prepared for use in lithium secondary batteries. The SiOC composite was synthesized by electrodeposition of $SiCl_4$. The composite anode delivered a discharge capacity of 1045 mA h per gram of Si at the 2000th cycle and 842 mA h per gram of Si even at the 7200th cycle. The reason for the excellent cyclability was investigated by methods including field emission scanning electron microscopy (FESEM), scanning transmission electron microscopy with an energy dispersive X-ray analyser (STEM-EDX), and X-ray photoelectron spectroscopy (XPS). The results revealed that the excellent cyclability was achieved by the homogeneous dispersion of SiO_x and organic/inorganic compounds at the nanometre scale. The structural uniformity of the SiOC composite is believed to have suppressed the crack formation attributable to the stress resulting from the reaction of silicon with lithium during charge–discharge cycles.

Introduction

Environmental issues such as global warming have become increasingly important in recent years, and the development of low-emission vehicles such as hybrid electric vehicles (HEVs) and battery-operated electric vehicles (BEVs) and the utilization of renewable energies have been attracting much attention.[1–3] The progress in portable electronic devices has also been significant. The development of these applications mainly depends on the advancement in the technology of energy storage, for which lithium ion batteries (LIB) are most suitable because of their high energy density and high power output.

The silicon anode system, along with the Sn anode system,[4–10] is promising because of the high theoretical capacity of 4200 mA h per gram of Si,[11,12] which is higher than that of graphite (372 mA h g^{-1}).

A long-life n-Si anode with 2000 mA h g^{-1} of capacity sustainable for more than 3000 cycles has been reported when the anode thickness was as thin as 50 nm.[13] In order to increase the capacity of the Si battery system, electrodes of thicker Si films were examined, but such electrodes did not hold their structure during charge–discharge cycles because of a large change in volume of the active material during the cycles.[14]

Waseda University, Faculty of Science and Engineering, 3-4-1, Okubo, Shinjuku-ku, Tokyo, Japan. E-mail: osakatets@waseda.jp; Fax: +81 3 3205 2074; Tel: +81 3 5286 3202

† Electronic supplementary information (ESI) available: Linear sweep voltammogram of the silicon deposition bath; potential profile during the silicon deposition; XRD pattern of the deposit prepared by the electrodeposition of silicon; GDOES depth profiles for the elements of Si, C, and O in the deposit; cyclic voltammogram for initial 3 cycles of the SiOC composite prepared by the electrodeposition of silicon. See DOI: 10.1039/c2ee03278c

Broader context

Lithium secondary batteries which are used in portable electric devices are important also in applications for electric vehicles and smart grids. The development of electric vehicles will be accelerated significantly by the reduction in size and weight of batteries, which, in turn, will be achieved by increasing the capacity of electrode materials. Silicon is a promising material because its theoretical capacity is ten times higher than that of carbon which is used as the conventional anode. However silicon has a critical problem of intrinsic expansion/contraction in volume during charge/discharge cycles, resulting in a rapid capacity fading attributed to a pulverization of anode. This problem impedes the practical use of silicon anodes. This paper describes results of our attempt to realize a practical silicon anode. Our silicon anode was prepared by an electrodeposition method, the technique of which was developed in the early 1800s. The silicon anode is composed of silicon oxide and carbon products produced during the electrodeposition (electrochemical reduction), which serve to buffer the stress attributed to the volume expansion/contraction of silicon. Consequently, the silicon anode delivers a capacity three times higher than that of the carbon anode with an outstanding cyclability of more than 7200 cycles.

To realize a long-life anode using Si, some attempts have been proposed, such as the introduction of core–shell structures,[15–18] a mesoporous structure,[19–21] and microstructures,[17,22–26] to prevent a decrease in paths of electricity during the operation. Recently, an electrodeposited Li–Si metallic anode was reported to show a capacity greater than 500 μA h cm^{-2}, which was retained for 50 cycles.[27] On the other hand, it has been reported that composites of SiO and carbon prepared by mechanical grinding showed a high capacity exceeding 3000 mA h g^{-1}.[28]

We recently proposed a novel SiOC composite for use as a Li battery anode. It was prepared by the electrodeposition from an organic solution.[29] The electrodeposition method was introduced based on the assumption that, to form a Si containing anode from an organic solution, the composite of Si with an organic/inorganic compound withstands the stress during the anode operation. Organic/inorganic compounds formed by the reduction of the organic solvent, as in the formation of a resultant solid electrolyte interphase (SEI) layer on anodes in Li ion batteries, are well known to exhibit permeability to Li^+ ions as well as chemical/electrochemical stability.[26,30–32] Based on these considerations, to realize a Si and organic/inorganic compound which would buffer the stress and exhibit Li^+ permeability, the electrochemical co-reduction of Si and the solvent was performed directly on the current collector. While there is a report on the Si related material formed by electrodeposition for the anode of Li batteries, their reversible capacity and cycle life are lower than those of the conventional carbon anode.[24] This paper introduces a silicon anode for lithium secondary batteries with an outstanding cycle durability.

Experimental

Preparation of the SiOC composite anode

$SiCl_4$ (Sigma-Aldrich), tetrabutylammonium perchlorate (TBAP, Kanto Chemical), propylene carbonate (PC, Kishida, H_2O content less than 30 ppm) and 1.0 mol dm^{-3} lithium perchlorate ($LiClO_4$)/PC–ethylenecarbonate (EC) (1 : 1 v/v) electrolyte solution (Kishida, H_2O content less than 20 ppm) were used without further purification. The electrolytic solution containing 0.5 mol dm^{-3} $SiCl_4$ and 0.5 mol dm^{-3} TBAP/PC for the deposition of the composite was prepared in dry air at the dew point lower than −50 °C. The electrochemical cell equipped with a Li reference electrode, 1.00 cm^2 Cu foil as a working electrode and a Pt counter electrode was set up in Ar atmosphere at the dew point lower than −90 °C. The Cu substrate was treated with 10% H_2SO_4 for 10 s, rinsed with distilled water, dried, and transferred into an Ar atmosphere. A constant cathodic current of 0.70 mA cm^{-2} was applied to pass a charge of 2.00 C cm^{-2} for the deposition.

Electrochemical measurement of the SiOC composite anode

The deposit on the Cu foil was transferred to an electrochemical cell equipped with a Li/Li^+ reference electrode containing 1.0 mol dm^{-3} $LiClO_4$/PC. The cell was charged and discharged by the constant-current (CC)–constant-voltage (CV) mode and by the CC mode, respectively, at 250 μA cm^{-2} in the potential range between 1.20 V and 0.01 V *vs.* Li/Li^+.

Characterization of the SiOC composite anode

The composite anode was characterized by means of field emission scanning electron microscopy with an energy dispersive X-ray analyser (FESEM-EDX, Hitachi, S-4800), scanning transmission electron microscopy with an EDX (STEM-EDX, Hitachi, HD-2700), glow discharge optical emission spectroscopy (GDOES, HORIBA, JY-5000RF), and X-ray photoelectron spectroscopy (XPS, JEOL, JPS-9010TR) after Ar^+ etching for 60 s was performed to remove the surface damaged during the transfer of the specimen into the chamber.

Results and discussion

To determine a proper set of conditions for the electrodeposition of silicon, linear sweep voltammetry was carried out with the electrochemical cell equipped with a Li reference electrode, a 1.00 cm^2 Cu foil as a working electrode and a Pt counter electrode in the electrolyte solution of 0.5 mol dm^{-3} $SiCl_4$ and 0.5 mol dm^{-3} TBAP in PC. The onset of the reductive current due to the decomposition of $SiCl_4$ was observed at *ca.* 1.3 V *vs.* Li (see ESI, Fig. S1†). The current density for the electrodeposition of silicon was adjusted to 0.7 mA cm^{-2} to maintain the potential during electrodeposition at *ca.* 1.3 V *vs.* Li. The discharge capacity of the electrodeposited silicon anode decreased with increasing current density during the electrodeposition of silicon. Therefore, the current density during the electrodeposition of silicon was set at 0.7 mA cm^{-2} in this investigation. The silicon electrodeposited in the PC solution with a charge of 2.00 C cm^{-2} was characterized.

The weight of deposits obtained by the electrodeposition of silicon was found to increase monotonically with increasing amount of passed charge. The weight of the deposit with a charge of 2.00 C cm^{-2} was found to be 105 μg on average, with an error of ±5 μg.

The SEM and STEM images of the deposit prepared by the electrodeposition of silicon are shown in Fig. 1. Fig. 1(a) shows a macroscopically homogeneous deposit. The parallel pattern on the deposit appears to have resulted from the pattern on the Cu foil substrate. The enlarged SEM image of Fig. 1(b) indicates that the deposit consisted of sub-micrometre clusters covering the Cu substrate with voids. The cross-sectional STEM image of the deposit (Fig. 1(c)) indicates the direct deposition on the Cu foil substrate. The thickness of the deposit corresponded approximately to the cluster size of approximately 0.5 μm.

The crystallinity of the deposit formed by the electrodeposition of silicon was investigated by XRD (see ESI, Fig. S2†). Two peaks were observed at *ca.* 50.5° and *ca.* 74.0°, which correspond to the peaks of Cu (200) and Cu (220), respectively. These peaks are due to the Cu foil substrate. Peaks expected for silicon, which are indicated in Fig. S2† by dotted lines, were not observed. This result suggests that the deposit formed by the electrodeposition of silicon was amorphous, which is supported by TEM analysis also. The existence of elemental silicon was confirmed by GDOES, XPS, and STEM-EDX. Fig. 2 shows the results of elemental mappings of the surface and the cross-section of the deposit obtained by SEM-EDX and STEM-EDX, respectively. Both the surface and cross-sectional elemental mapping show that Si, O, and C were distributed homogeneously at the nanometric scale. In cross-sectional images, Si, O, and C were detected

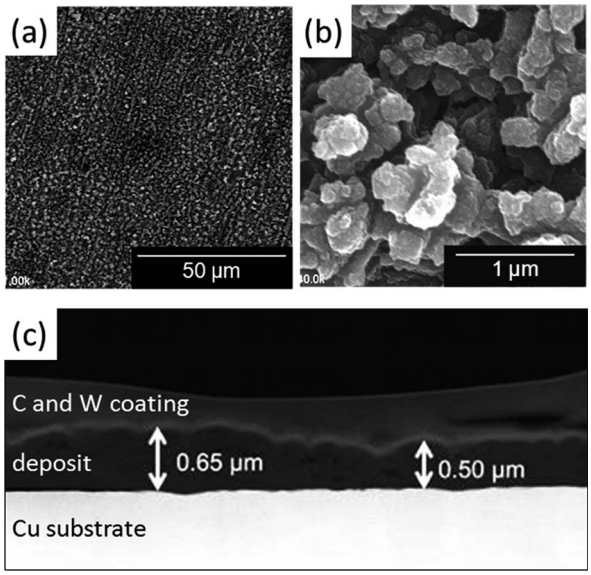

Fig. 1 Plane view FESEM image (a), enlarged image (b), and cross-sectional STEM image (c) of the deposit prepared by the electrodeposition of silicon.

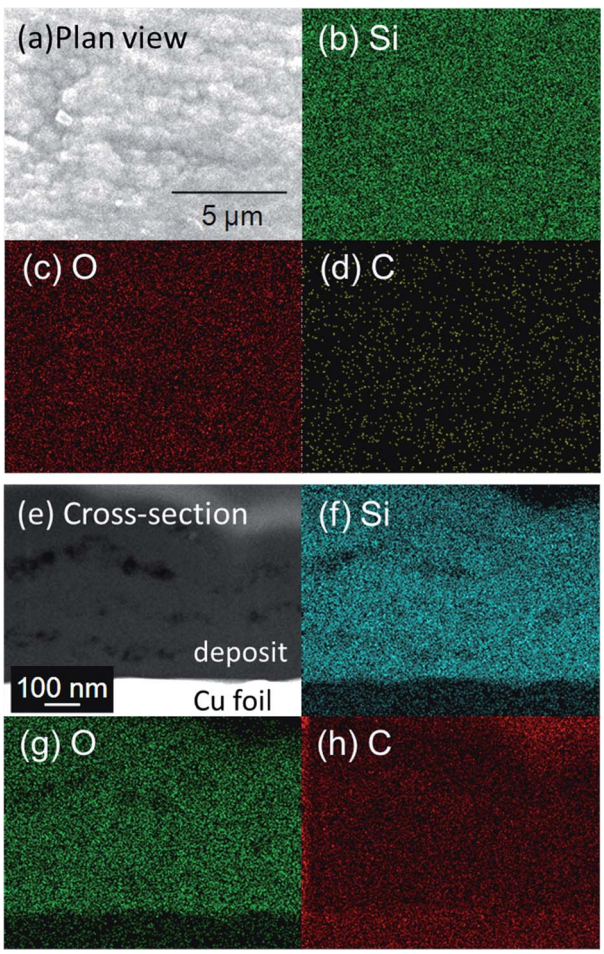

Fig. 2 Plane view SEM image (a) and elemental mappings of Si (b), O (c), and C (d), and cross-sectional STEM image (e), and element mappings of Si (f), O (g), and C (h).

on the Cu foil substrate, because Si, O, and C were spattered by focused ion beams for the preparation of the STEM specimens. The results of the XRD and EDX revealed the deposit to be an amorphous composite of Si, O, and C with nano-scale dispersion.

XPS spectra of the deposit obtained by the electrodeposition of silicon are shown in Fig. 3(a)–(c). Peaks attributable to $Si_{2p3/2}$, O_{1s}, and C_{1s} were observed. The spectrum of $Si_{2p3/2}$ revealed that the peak is located at the binding energy of about 103 eV, which indicates that the electronic state of Si is SiO_x instead of Si metal whose peak would appear at about 99 eV.[33–36] In the O_{1s} spectrum of the as-formed deposit, a peak was observed at about 532.2 eV, as represented by the oxygen in the state of C–O–C. This peak may consist of overlapped peaks for C–O–Si and Si–O–Si.[33] In the C_{1s} spectrum of the as-formed deposit, a peak was observed at about 284 eV, as represented by the carbon in the C–C bond.[37] The C–O–C and C–C bonds are attributed to decomposition products of the organic electrolyte formed during the silicon deposition. The results of XPS indicate that the deposit was composed of Si existing in an oxidized state and decomposition products of the organic electrolyte.

GDOES depth profiles of the elements of Si, C, and O in the deposit obtained by the electrodeposition of silicon are shown in Fig. S3†. The silicon content was found to increase with depth near the surface, and saturate at *ca.* 60 wt%. The carbon and oxygen contents were found to decrease with depth near the surface to saturate at *ca.* 22 wt% and *ca.* 17 wt%, respectively. These tendencies near the surface are attributed to the measurement process, *i.e.*, the oxidation by exposure in air, and the heterogeneous surface of the deposit as shown in Fig. 1(b). Hence, the composition of the deposit was determined to be Si/C/O = 61.6/21.8/16.6 by weight from the composition at the depth of 1.0 to 1.5 μm. Considering the GDOES result, the weight of silicon in the deposit prepared with a charge of 2.00 C cm^{-2} was *ca.* 64.5 μg. Therefore, the efficiency of silicon deposition, which is a 4-electron reaction as indicated in eqn (1), was calculated to be 44.4%. The result also indicates decomposition of the organic electrolyte during the silicon deposition, resulting in the formation of SiOC composite.

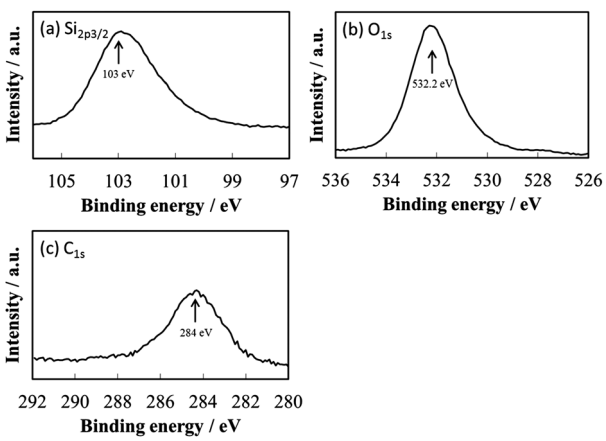

Fig. 3 XPS spectra obtained with deposit sample. The surface layer was etched by Ar^+ for 60 s. The spectra of $Si_{2p3/2}$, O_{1s}, and C_{1s} are shown in (a), (b), and (c), respectively.

$$SiCl_4 + 4e^- \rightarrow Si + 4Cl^- \quad (1)$$

Electrochemical performance of the SiOC composite as an anode of a Li battery was examined by a CC–CV charge (lithiation)–CC discharge (delithiation) test. Fig. 4(a) shows the potential profiles during the charge–discharge test. In the initial lithiation process, a negative potential overshoot was observed due to the nucleation of a new phase, that is the Li_2O phase.[38] The capacity for the first lithiation was 4731 mA h g^{-1}, while the capacity for the first delithiation was 1403 mA h g^{-1}. The large irreversible capacity is attributed mainly to the conversion reaction of SiO_x to $SiLi_y$ and Li_2O,[38,39] and partly due to SEI formation,[16,26,32] which is indicated by the potential plateau above 0.4 V *vs.* Li/Li^+ in Fig. 4(a) and the reductive current above *ca.* 0.4 V *vs.* Li/Li^+ in the first cathodic scan of the cyclic voltammogram (see ESI, Fig. S4†). In the first discharge, the potential plateau for delithiation below 0.6 V *vs.* Li/Li^+ was confirmed, which corresponds to the anodic peaks repeated at 0.32 and 0.46 V *vs.* Li/Li^+ in the cyclic voltammogram (Fig. S4†), whose result accords with the delithiation of silicon.[40] After the 1st cycle, the SiOC anode was charged at a potential below 0.3 V *vs.* Li/Li^+, and discharged at a potential plateau below 0.6 V *vs.* Li/Li^+. At the initial stage of charging in each cycle for 300 cycles, the electrode potential dropped at the beginning to about 0.2 V *vs.* Li/Li^+ and then decreased while the current was being passed.

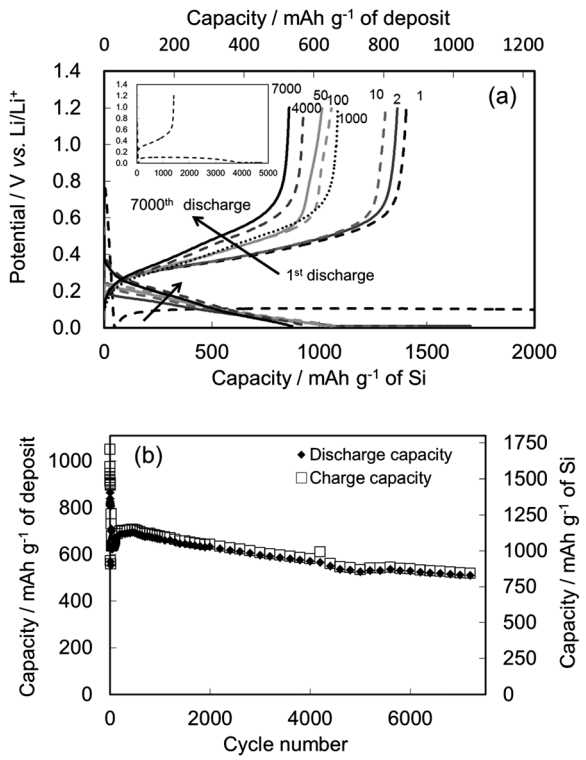

Fig. 4 Potential profiles of the SiOC composite anode for Li batteries during charge–discharge cycling at various cycle numbers (a) and plots of charge–discharge capacity against the number of cycles (b). The inset in (a) indicates the potential profiles during the first lithiation and delithiation. The capacity values were normalized with respect to the weight of initial deposit or the calculated amount of Si in the deposit. The applied current density was 250 μA cm^{-2} (1.0 C-rate).

With increasing number of cycles, the initial potential shifted towards 0.4 V *vs.* Li/Li^+. After the 300th cycle, the potential profile during the charging did not change significantly. The potential profiles during discharge were identical in all stages except for the amount of discharge capacity. The value of discharge capacity was found to be above 1000 mA h g^{-1} of Si or above 630 mA h g^{-1} of the deposit even after 2000 cycles. The decrease was gradual. The discharge capacity of 1000 mA h g^{-1} corresponds to a value as high as 0.238 C cm^{-2} for the electrode examined in this study. Fig. 4(b) reveals clearly the capacity value of the composite under a loading current of 250 μA cm^{-2}, which corresponds to a value of 1.0 in the C-rate. At the initial stage the composite exhibited a high value above 1200 mA h g^{-1} of Si. After the 50th cycle, the value increased beyond 1100 mA h g^{-1} of Si and showed a gradual decrease while the discharge capacity kept a value higher than 1000 mA h g^{-1} of Si for more than 2000 cycles. These results show that the composite was formed by the reduction of $SiCl_4$ followed by the initial reduction process, and that Si oxide may not have been reduced completely. The remaining Si oxides are considered to have been reduced during the charging steps of the cycling test. This conversion reaction led to an increase in the amount of active Si and the discharge capacity in the early stages of the cycling test. Also, successive phase transition between Si and SiLi alloy during the charge–discharge cycles may lead to the formation of electronic pathways and/or ionic pathways in the anode matrix.

The columbic efficiency in charge–discharge cycling was found to be higher than 98%, except for several initial cycles. The low efficiency in the first cycle may be due to the consumption of reducing charge for Si oxide remaining after the initial reduction process, as discussed above. The effect of completion of the conversion explains the potential decay in the first stage of charging up to 300 cycles. The electrode potential at the beginning of the charging process shifted from 0.2 V to 0.4 V *vs.* Li/Li^+ over 300 cycles. It is considered that, at the initial stages, adequate conduction pathways for electrons and/or Li^+ ions were not formed within the anode matrix. During the continuous charge–discharge cycles, with the further reduction of Si oxide and a succession of phase conversion between Si–Li and Si, a combination with the Si phase may take place to allow for maintaining adequate electric conduction pathways or ionic transportation pathways within the anode matrix.

The anodes being cycled at 1.0 C-rate exceeded 7200 cycles with a discharge capacity of 842 mA h g^{-1} of Si. By utilizing such an anode material having a capacity of 1000 mA h g^{-1}, it becomes possible to increase the capacity by *ca.* 20% for the entire battery as compared with a battery using a conventional carbon anode material. While there were some experimental deviations in the capacity profiles at the initial stages, the electrochemically formed SiOC composite was revealed to have a very long cycle life with a discharge capacity higher than 1000 mA h g^{-1} of Si.

The plane view FESEM images of an SiOC anode after the first lithiation are shown in Fig. 5(a) and (b). After the first lithiation, the voids observed in the SiOC composite before the first lithiation decreased. This is attributed to the expansion of silicon by lithiation and also to SEI formation as seen in Fig. 4(a). The thickness of the SiOC composite after the first lithiation was found to be *ca.* 3.3 μm on average from the STEM image shown in Fig. 5(c). Thus, it was suggested that the SiOC

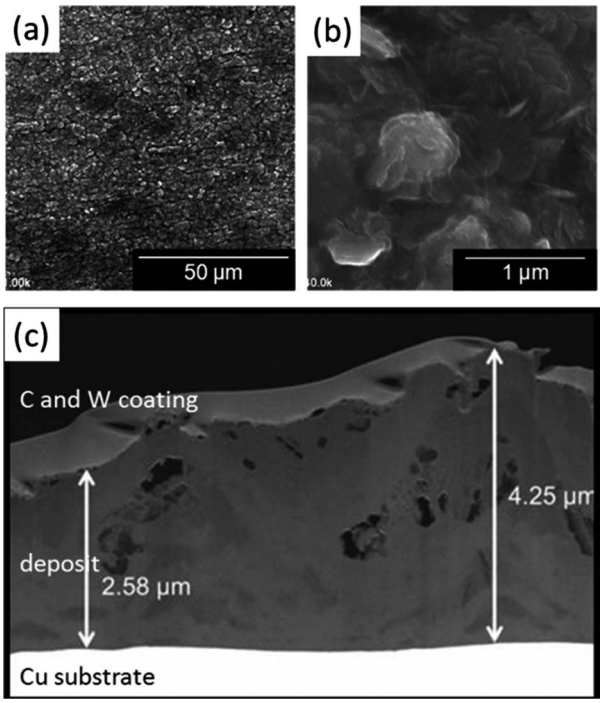

Fig. 5 Plane view FESEM image (a), enlarged image (b), and cross-sectional STEM image (c) of the SiOC anode after the first lithiation.

composite anode expanded after the first lithiation because of the reaction of silicon with lithium and the SEI formation.

The potential during the operation of anodes, such as tin and silicon, is close to the potential of metallic lithium, where almost no solvent or salt can be thermodynamically stable. Hence, organic electrolytes undergo electrochemical decomposition resulting in the formation of a passive SEI, through which lithium ions can migrate but electrons cannot penetrate.[26,32] The SEI layer on silicon electrodes in alkyl carbonate electrolytes is reported typically to consist of a heterogeneous mosaic of composites including polyethylene oxide, lithium alkyl carbonate ($R–CH_2OCO_2Li$), lithium alkoxides (ROLi), lithium carbonate (Li_2CO_3), lithium oxide (Li_2O), and silicon species.[16,26,37,41]

The XPS spectra of the SiOC anode after the first lithiation and after 100 cycles are shown in Fig. 6 to reveal the variation of the SiOC anode brought about by charge–discharge cycling. In the SiOC anodes after the first lithiation and after 100 cycles, peaks attributed to $Si_{2p3/2}$, O_{1s}, C_{1s}, and Li_{1s} were observed. The peak of $Si_{2p3/2}$ observed before the first lithiation shifted to a lower binding energy of *ca.* 101.5 eV, which suggests that the Si was partially reduced,[34,36] which also indicates the occurrence of the conversion reaction of SiO_x.[42] The peak of O_{1s} with a height of *ca.* 531 eV and a shoulder at *ca.* 529.5 eV implies the existence of Li_2CO_3, LiOH, and Li_2O,[37,43,44] besides Li_4SiO_4, which might have been formed as reported by Guo *et al.*[42] In the spectrum of C_{1s}, a peak appeared at about 289 eV after the first lithiation. This peak suggests the formation of carbonates including Li_2CO_3 and $R–CH_2OCO_2Li$.[43,45] In the spectrum of Li_{1s}, the broad peak at about 54.5 eV implies the formation of Li_2O, Li_2CO_3, and LiOH,[43,46,47] in accord with the results of the peak of O_{1s}. The existence of Li_2O was supported by TEM analysis (not shown). The spectra of $Si_{2p3/2}$, O_{1s}, C_{1s}, and Li_{1s} after 100 cycles were

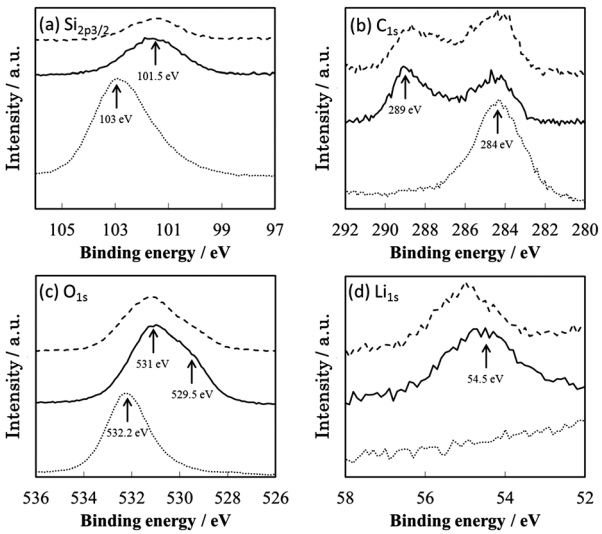

Fig. 6 XPS spectra of SiOC anodes after the first lithiation (solid line) and after 100 cycles (dashed line) obtained with samples with the surface layer etched by Ar^+ for 60 s. The spectra of $Si_{2p3/2}$, C_{1s}, O_{1s}, and Li_{1s} are shown in (a), (b), (c), and (d), respectively. For comparison, XPS spectra of the SiOC anode before the first lithiation are indicated by dotted lines, as in Fig. 3.

essentially unchanged from the spectra after the first lithiation. The increase of the content of Li_2CO_3 was confirmed by TEM analysis (not shown). Thus, the results of XPS analysis suggest that the SEI is formed on the SiOC anode after the first lithiation and is almost retained after 100 cycles.

The morphology of the SiOC anode surface was examined after 10 and 300 cycles to find the reason why the excellent cycle durability was achieved. The FESEM images of SiOC anodes after the 10^{th} and the 300^{th} cycles are shown in Fig. 7. The particles observed on the SiOC anode surface after the first lithiation were absent after the 10^{th} cycle. This phenomenon must be due to the progress of SEI formation, which is evidenced by the lower columbic efficiency during the initial cycles (Fig. 4). The cracking of the SiOC anode caused by the large volume

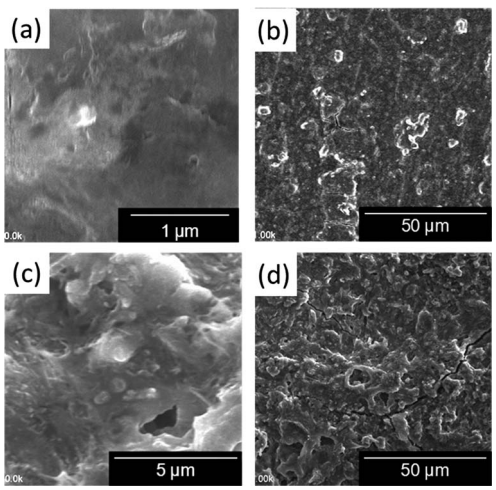

Fig. 7 Plane view FESEM images of SiOC anodes after the 10^{th} cycle (a) and (b), and after the 300^{th} cycle (c) and (d).

change of silicon, which is a problem associated with the Si anode system,[14,48,49] was not observed. This is attributed to a uniform reaction of the well-dispersed SiO_x at the nanometre scale as confirmed by STEM-EDX (Fig. 2) and to the buffering effect of products of the decomposition of the organic solvent. After the 100th cycle, although cracking was observed to a slight extent, the surface morphology was almost unchanged even after the 300th cycle. The results of the FESEM observation imply that the suppression of crack formation leads to the excellent cycle durability of the SiOC anode.

Conclusions

On the basis of the assumption that the composite of Si with an organic/inorganic compound withstands the stress associated with the anode operation, a homogeneous SiOC composite at the nanometre scale was successfully formed directly on a Cu substrate by electrodeposition in a PC solution containing $SiCl_4$.

The SiOC composite anode exhibited an outstanding durability against charge–discharge cycles and delivered the discharge capacity of 1045 mA h g^{-1} at the 2000th cycle and 842 mA h g^{-1} of Si even at the 7200th cycle. These superior results were achieved by the uniform dispersion of SiO_x in the organic/inorganic compound synthesized by the electrodeposition of silicon in an organic solvent, which were confirmed by STEM-EDX and XPS. The reasons why the SiOC composite anode withstood thousands of cycles were discussed from the standpoint of the crack formation attributed to the reaction of silicon with lithium during charge and discharge cycles.

Acknowledgements

This work was supported partly by "Research & Development Initiative for Scientific Innovation of New Generation Batteries (RISING)" from the New Energy and Industrial Technology Development Organization (NEDO), Japan, and partly by the Grant-in-Aid for Specially Promoted Research "Establishment of Electrochemical Device Engineering" from the Ministry of Education, Culture, Sports, Science and Technology, Japan. This work was done at the Global COE Program "Center for Practical Chemical Wisdom".

Notes and references

1 J. B. Goodenough and Y. Kim, *Chem. Mater.*, 2010, **22**, 587–603.
2 C. Liu, F. Li, L. P. Ma and H. M. Cheng, *Adv. Mater.*, 2010, **22**, E28–E62.
3 B. Scrosati and J. Garche, *J. Power Sources*, 2010, **195**, 2419–2430.
4 K. E. Aifantis, S. Brutti, S. A. Hackney, T. Sarakonsri and B. Scrosati, *Electrochim. Acta*, 2010, **55**, 5071–5076.
5 J. Hassoun, G. A. Elia, S. Panero and B. Scrosati, *J. Power Sources*, 2011, **196**, 7767–7770.
6 H. Mukaibo, T. Momma, M. Mohamedi and T. Osaka, *J. Electrochem. Soc.*, 2005, **152**, A560–A565.
7 H. Mukaibo, T. Momma and T. Osaka, *J. Power Sources*, 2005, **146**, 457–463.
8 H. Mukaibo, T. Osaka, P. Reale, S. Panero, B. Scrosati and M. Wachtler, *J. Power Sources*, 2004, **132**, 225–228.
9 H. Mukaibo, A. Yoshizawa, T. Momma and T. Osaka, *J. Power Sources*, 2003, **119**, 60–63.
10 H. Nara, Y. Fukuhara, A. Takai, M. Komatsu, H. Mukaibo, Y. Yamauchi, T. Momma, K. Kuroda and T. Osaka, *Chem. Lett.*, 2008, 142–143.
11 S. Bourderau, T. Brousse and D. M. Schleich, *J. Power Sources*, 1999, **81**, 233–236.
12 W. J. Weydanz, M. Wohlfahrt-Mehrens and R. A. Huggins, *J. Power Sources*, 1999, **81**, 237–242.
13 T. Takamura, S. Ohara, M. Uehara, J. Suzuki and K. Sekine, *J. Power Sources*, 2004, **129**, 96–100.
14 U. Kasavajjula, C. Wang and A. J. Appleby, *J. Power Sources*, 2007, **163**, 1003–1039.
15 L. F. Cui, R. Ruffo, C. K. Chan, H. L. Peng and Y. Cui, *Nano Lett.*, 2009, **9**, 491–495.
16 Y. C. Yen, S. C. Chao, H. C. Wu and N. L. Wu, *J. Electrochem. Soc.*, 2009, **156**, A95–A102.
17 L. Ji, Z. Lin, M. Alcoutlabi and X. Zhang, *Energy Environ. Sci.*, 2011, **4**, 2682–2699.
18 B. Scrosati, J. Hassoun and Y.-K. Sun, *Energy Environ. Sci.*, 2011, **4**, 3287–3295.
19 W. Chen, Z. L. Fan, A. Dhanabalan, C. H. Chen and C. L. Wang, *J. Electrochem. Soc.*, 2011, **158**, A1055–A1059.
20 J. Cho, *J. Mater. Chem.*, 2010, **20**, 4009–4014.
21 H. Kim and J. Cho, *Nano Lett.*, 2008, **8**, 3688–3691.
22 H. Kim, B. Han, J. Choo and J. Cho, *Angew. Chem., Int. Ed.*, 2008, **47**, 10151–10154.
23 A. Magasinski, P. Dixon, B. Hertzberg, A. Kvit, J. Ayala and G. Yushin, *Nat. Mater.*, 2010, **9**, 353–358.
24 M. Schmuck, A. Balducci, B. Rupp, W. Kern, S. Passerini and M. Winter, *J. Solid State Electrochem.*, 2010, **14**, 2203–2207.
25 L. Ji and X. Zhang, *Energy Environ. Sci.*, 2010, **3**, 124–129.
26 J. R. Szczech and S. Jin, *Energy Environ. Sci.*, 2011, **4**, 56–72.
27 R. Lv, J. Yang, J. Wang and Y. Nuli, *J. Power Sources*, 2011, **196**, 3868–3873.
28 M. Yamada, A. Ueda, K. Matsumoto and T. Ohzuku, *J. Electrochem. Soc.*, 2011, **158**, A417–A421.
29 T. Momma, S. Aoki, H. Nara, T. Yokoshima and T. Osaka, *Electrochem. Commun.*, 2011, **13**, 969–972.
30 P. Verma, P. Maire and P. Novak, *Electrochim. Acta*, 2010, **55**, 6332–6341.
31 M. Winter, W. K. Appel, B. Evers, T. Hodal, K. C. Moller, I. Schneider, M. Wachtler, M. R. Wagner, G. H. Wrodnigg and J. O. Besenhard, *Monatsh. Chem.*, 2001, **132**, 473–486.
32 K. Xu, *Energies*, 2010, **3**, 135–154.
33 Q. Xia, B. Wang, Y. P. Wu, H. J. Luo, S. Y. Zhao and T. van Ree, *J. Power Sources*, 2008, **180**, 602–606.
34 C.-M. Park, W. Choi, Y. Hwa, J.-H. Kim, G. Jeong and H.-J. Sohn, *J. Mater. Chem.*, 2010, **20**, 4854–4860.
35 R. Alfonsetti, L. Lozzi, M. Passacantando, P. Picozzi and S. Santucci, *Appl. Surf. Sci.*, 1993, **70–71**(Part 1), 222–225.
36 C. D. Wagner, D. E. Passoja, H. F. Hillery, T. G. Kinisky, H. A. Six, W. T. Jansen and J. A. Taylor, *J. Vac. Sci. Technol.*, 1982, **21**, 933–944.
37 C. K. Chan, R. Ruffo, S. S. Hong and Y. Cui, *J. Power Sources*, 2009, **189**, 1132–1140.
38 A. Netz, R. A. Huggins and W. Weppner, *J. Power Sources*, 2003, **119–121**, 95–100.
39 H. Robert, *Solid State Ionics*, 1998, **113–115**, 57–67.
40 T. Jiang, S. Zhang, X. Qiu, W. Zhu and L. Chen, *Electrochem. Commun.*, 2007, **9**, 930–934.
41 S. W. Song and S. W. Baek, *Electrochem. Solid-State Lett.*, 2009, **12**, A23–A27.
42 B. Guo, J. Shu, Z. Wang, H. Yang, L. Shi, Y. Liu and L. Chen, *Electrochem. Commun.*, 2008, **10**, 1876–1878.
43 D. Aurbach, I. Weissman, A. Schechter and H. Cohen, *Langmuir*, 1996, **12**, 3991–4007.
44 L. Chen, K. Wang, X. Xie and J. Xie, *J. Power Sources*, 2007, **174**, 538–543.
45 S. H. Kang, D. P. Abraham, A. Xiao and B. L. Lucht, *J. Power Sources*, 2008, **175**, 526–532.
46 K. Kanamura, H. Tamura, S. Shiraishi and Z. I. Takehara, *Electrochim. Acta*, 1995, **40**, 913–921.
47 K. Kanamura, H. Tomura, S. Shiraishi and Z. I. Takehara, *J. Electrochem. Soc.*, 1995, **142**, 340–347.
48 S.-J. Lee, J.-K. Lee, S.-H. Chung, H.-Y. Lee, S.-M. Lee and H.-K. Baik, *J. Power Sources*, 2001, **97–98**, 191–193.
49 H. Li, X. Huang, L. Chen, Z. Wu and Y. Liang, *Electrochem. Solid-State Lett.*, 1999, **2**, 547–549.